Influence of hydrogen addition on methane coupling in a moderate pressure microwave plasma

M. Wnukowski[a]*, A.W. van de Steeg[b], B. Hrycak[c], M. Jasiński[c], G.J. van Rooij[b]

[a] - Wroclaw University of Science and Technology, Faculty of Mechanical and Power Engineering, Wybrzeże Stanisława Wyspiańskiego 27, 50-370 Wrocław, Poland

[b] - Dutch Institute for Fundamental Energy Research (DIFFER), De Zaale 20, Eindhoven 5612 AJ, the Netherlands

[c] - Institute of Fluid Flow Machinery, Polish Academy of Sciences, Fiszera 14, 80-231 Gdańsk, Poland

* - corresponding author: mateusz.wnukowski@pwr.edu.pl

Abstract

In this paper, the effect of hydrogen addition on methane coupling in a microwave moderate pressure (55 mbar and 110 mbar) plasma reactor has been studied. The use of optical emission spectroscopy allowed the determination of the rotational temperature of heavy particles and showed it to be in the range of 3000- 4000 K. Due to the high temperature in the discharge the dominant product was acetylene and it was concluded that the methane coupling process is mainly through thermal decomposition with a key role of H radicals. It was revealed that the addition of hydrogen can increase both methane conversion and acetylene and ethylene yield and selectivity. With the CH_4:H_2 ratio of 1:1, the methane conversion increased from 31.0% to 42.1% (55 mbar) and from 34.0% to 48.6% (110 mbar), when compared to pure methane plasma. Respectively, the yield of acetylene increased from 14.4% to 25.3% (55 mbar) and from 20.1% to 34.0% (110 mbar). Moreover, the addition of hydrogen decreased the output of the problematic soot-like product. These results indicate that hydrogen addition can be a simple yet effective method of increasing selectivity to desirable products in plasma reforming of CH_4.

Keywords: Methane coupling; Microwave plasma; Hydrogen; Ethylene; Acetylene

1. Introduction

Methane is believed to play a key role as a hydrocarbons feedstock in the near future [1–3]. One of the main reasons is that, as opposed to depleting crude oil reserves that are commonly used in the petrochemical industry, the number of methane sources is constantly increasing (new deposits of natural gas and alternative sources of methane) [1,2]. As a result, much effort is put into developing a process that allows for efficient methane conversion, especially to valuable C_2 products (C_2H_2 and C_2H_4) that are commonly used as feedstock in the chemical industry [4–6].

Despite the scientific attention given, no significant industrial-scale breakthrough has been achieved in that matter yet. Conversion of methane to valuable chemicals can be done by indirect routes involving multiple steps, i.e. via production of synthetic gas or methanol, that further can be processed into olefins [7]. The main drawback of such a process is the complexity, leading to high costs and the usual need for additional H_2. Moreover, with the hydrogen being produced coming mainly from fossil fuels by steam reforming, these methods would contribute greatly to CO_2 emission.

Another possible process of C_2 compounds production is oxidative methane coupling (OMC). While this process has been intensively investigated over the last 20-30 years the main problematic issue - providing a perfect catalyst - remains unsolved [7,8]. This issue is connected with oxidation of methane, resulting in formation of CO_2, which is competitive to C_2 production [9,10]. Moreover, the secondary problem is the stability of the catalyst and its sintering in the high temperature of the process [8,11] as well as the need for an expensive oxygen/nitrogen separation [8,10].

With the European Green Deal, focusing on CO_2 reduction, being implemented and the unavoidable shortage of oil reserves, the direct non-oxidative methane coupling into C_2 compounds might become a highly desired process in the near future. However, conventional processes of thermal methane coupling are limited by the high energy required to activate the stable methane molecule [5,7]. Additionally, these processes suffer from a few other drawbacks, like catalyst deactivation in the presence of soot, long start-up/shut-down periods, low energy efficiency, and indirect CO_2/NO_x production [5].

In that context, plasma non-oxidative methane coupling is considered as a promising method of C_2 compounds production. Plasma provides a high concentration of chemically active species that can enhance methane activation. Moreover, plasma reactors have a low inertia and can be started /shut-down quickly all the while being considered CO_2 neutral if powered with renewable energy. Plasma driven methane activation can be done in both thermal and non-thermal plasma; the thermal plasma, for example the Hüels process, is characterized by low energy efficiency and the need of intensive quenching [10,12,13]. A suitable alternative could be found in non-thermal plasma. Many non-equilibrium plasmas are described extensively in literature in the context of methane coupling [5,14,15]: dielectric-barrier discharge (DBD) [16–19], nanosecond pulsed discharge (PD) plasma [1,6,20,21], glow discharge [22,23], corona plasma [24,25], gliding-arc (GA) plasma [4,26,27] and microwave (MW) plasma [5,10,28]. Of these plasma sources, MW plasma is often claimed to show the highest rate and energy efficiency of methane conversion. The MW plasma parameters can vary in a wide range from strictly non-equilibrium to close to thermal

equilibrium depending on the operating pressure and power [5]. Regardless of the condition, the temperature within the methane plasma is usually above 1000-2000 K [10,29] providing a suitable condition for methane decomposition through thermal chemistry, thereby reaching conversions above 80% and maintaining high selectivity towards C_2 compounds [14]. The MW plasma can be considered a warm plasma [26,30], meaning, that despite the high temperature it can still show a vibrational non-equilibrium of its particles. In fact, some authors have stated that this non-equilibrium, as a result of vibrational excitation of methane, can enhance its decomposition [4,10,16,31,32]. However, experimental validation of vibrational non-equilibrium and its role in dissociation of methane was often lacking [14,32,33]. Moreover, recent research in this field suggests, that in fact this phenomenon is rather negligible in the commonly used experimental plasma reactors (including MW plasma), and the process of methane conversion is thermally driven [14,33]. Nevertheless, applying MW plasma can also be beneficial from a technical point of view. Magnetrons used in microwave plasma generation are the same as those used in other industrial applications of microwaves, which are considered to be mature technologies, e.g. drying, food processing, and heating in general [34]. Microwave technology elements are relatively cheap and have a simple and compact construction [35], they are produced by many companies and their power can vary from few to hundreds of kW, creating the potential to scale up the technology.

Regardless of the method applied for methane coupling, one of the main, unavoidable products is hydrogen. Interestingly, the addition of hydrogen into the methane gas stream can significantly affect the process, i.e. methane conversion rate and distribution of the products. This effect can be twofold. In high temperature conditions, as in warm microwave plasma, the addition of hydrogen can result in the presence of additional highly energetic H radicals that can enhance methane conversion [36]. On the other hand, typical for conventional thermal pyrolysis of methane or strictly non-thermal plasmas [5,37], the addition of hydrogen can result in both a lower conversion, due to methyl radical recombination into methane, as well as suppression of benzene and soot production by inhibition of acetylene decomposition. However, these two effects are not always contradicting. In works where atmospheric MW plasma was studied, a high hydrogen dilution (e.g. CH_4:H_2 ratio above 1:1) resulted in both increasing methane conversion and C_2 compounds yield as well as inhibiting soot production [2,3].

Despite the promising potential of MW plasma application in methane coupling and the possible benefits of hydrogen addition, the amount of works focusing on this issue is limited. The two prominent works in that field are the work of Heintze et al. [38] and the work of Shen et al. [3]. The first work used a moderate pressure (30 mbar) MW plasma and therein focused on the

mechanism behind C_2 compound formation and the effect of H-atoms on it. The H_2 addition was limited to only 17% v/v. The latter work used an atmospheric MW plasma reactor and studied a wide range of CH_4:H_2 ratios (from 5:1 to 1:5) in order to find the effect of H_2 addition on methane conversion and product distributions. This work lacked any information considering plasma parameters, and the mechanisms behind the hydrogen addition were only briefly discussed. Taking into account the limited literature data and the variety of possible process conditions (i.e. MW plasma pressure and temperatures, hydrogen dilution), this work aims to investigate the impact of hydrogen addition (CH_4:H_2 ratios of 3:1 and 1:1) on methane coupling in a moderate pressure (55 mbar and 110 mbar) MW plasma reactor. The work involves the determination of the methane conversion products along with the investigation of the plasma temperatures.

2. Material and methods

2.1. Experimental setup

The experimental layout is schematically shown in Fig. 1. A magnetron power source (IBF PGEN2450/1-2KW5CSW) applies microwaves of up to 1000 W peak power via a WR340 waveguide to a 27 mm inner diameter quartz tube, where the plasma is generated. An EH tuner and an adjustable short are used to tune the electrical field for minimal reflected power. Gas is injected tangentially, which is a common design in MW plasma reactors [29,39]. The tangential injection creates a vortex in the quartz tube which stabilizes the plasma in the center and prevents the walls of the reactor from coming into contact with the plasma [40]. The pressure and velocity in the reactor center are lower than at the wall [41], two effects that ensure the ignition is favored in the tube center. At the wall, the pressure and velocity are higher leading to better cooling of the discharge tube. Lack of the swirl would impede the ignition of the discharge and leave the quartz tube vulnerable to the high plasma temperatures, which eventually would melt the quartz.

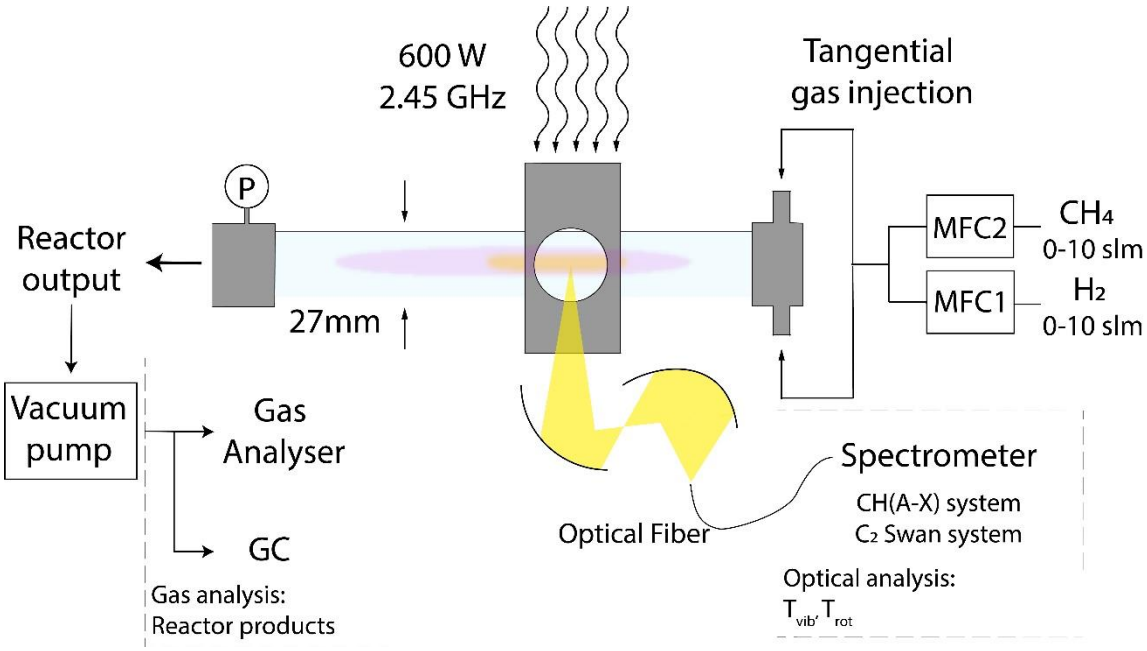

Fig. 1. Schematic overview of the complete reactor system. MFCs regulate gas flow to a tangential gas injection manifold, creating a swirl flow in the quartz tube. Microwave power is applied through WR340 waveguides, creating a plasma in the center of the quartz tube. Emission of the center of the plasma is imaged into an optical fiber connected to a spectrometer for optical emission measurements. Downstream of the plasma pressure is registered, and a gas analyzer is connected after the vacuum pump for H_2 measurements. Samples for gas-chromatograph measurements can be taken from the exhaust.

The flow rates of the gases used during the experiments were controlled with the use of mass flow controllers (MFC) (Tylan 2900 for hydrogen and Bronkhorst EL-FLOW F-201AV for methane) with the total flow kept constant at 6 SLM (standard liter per minute). The changes in the volumetric gas flow rate occurring during the process were measured with the use of a gas meter (G1.6, Metrix) connected to the exhaust of the vacuum pump (Edwards XDS35i). Alternatively, the outlet of the setup could have been connected to the gas analyzer or Tedlar's bags used for gas sampling. Pressure was recorded by an MKS Instruments 910 DualTrans gauge, located 20 cm downstream of the quartz tube.

2.2. Methodology

2.2.1. Process parameters

On the base of previous research [10] and preliminary tests with different sets of power, gas flow rate, and pressure, it was decided to work with the total gas flow rate of 6 SLM, the microwave power of 600 W (with the socket power of the MW source being 1000 W), and two pressures: 55 mbar and 110 mbar. These two sets were selected as they provided a noticeable and similar conversion of methane with a distinctively different ethylene output and plasma shape. The plasma shape is significantly altered due to a change in operating mode: radial confinement takes

place, empirically seen to occur around 100 mbar. The contraction mechanics of methane are not well characterized, and neither is the effect of contraction on reactor output and product selectivity, for which we provide a first characterization in this work. For the two mentioned pressures, the 55 mbar plasma resulted in a diffuse shape while at 110 mbar the plasma was radially confined to a bright filament. From other molecular plasma, it is expected the confinement to be accompanied by a local higher temperature and dissociation degree [42]. If this holds for methane it is thus expected to alter the product distributions accordingly. Finally, within these two sets of parameters, hydrogen was added to the gas mixture. The gas flow rates of methane and hydrogen were changed to provide the following CH_4:H_2 ratios: 1:0, 3:1 and 1:1. Higher ratios were not possible to achieve due to problems with plasma stability. With higher hydrogen content the swirl flow could no longer stabilize the plasma, leading to strong heat fluxes to the quartz tube and subsequent melting of the reactor. It should be noted that the referred work [10] also discusses the influence of a flow rate and input power on the methane conversion process which is not in the scope of this work.

2.2.2. Gas analysis

The concentration of hydrogen was measured online with the use of analyzer (GAS 3100 Syngas Analyzer, GEIT), connected to the outlet of the vacuum pump, equipped with a thermal conductivity detector. The rest of the products were determined with the use of gas chromatography (GC) techniques. The GC analyses were done with the use of outlet gas samples collected in the Tedlar's bags. The samples were analyzed with the use of mass spectrometry (GC-MS) (7820 with MSD 5977, Agilent) for the purpose of qualitative analysis, and with the use of flame-ionized detector (GC-FID) (6890, Hewlett-Packard) for the quantitative analysis. The quantitative analysis was based on methane and acetylene calibration curves and the fact that the FID response is proportional to the concentration and number of C atoms in the molecule [43]. Additionally, the qualitative analysis was supported by the comparison of the GC-FID results with the standard column chromatogram provided by the column producer. More information on the columns used and the GC conditions are given in Table 1.

Table 1. GC methods applied in the experiment.

Detector	Column	Carrier gas	Temperature program	Purpose
MS	HP-PLOT Q (Agilent J&W) 30m x 0.320mm x 20µm	He, 1 ml/min split: 50	60°C (5 min) $\xrightarrow{10°C/min}$ 180°C (8 min)	Qualitative
FID	RT-Alumina BOND/KCl (Restek) 50m x 0.530mm x 10µm	H_2, 8 psi split: 5	45°C (1 min) $\xrightarrow{10°C/min}$ 200°C (3.5 min)	Qualitative

FID	RT-Alumina BOND/KCl (Restek) 50m x 0.530mm x 10µm	H_2, 8 psi split: 5	100°C (20 min)	Quantitative

2.2.3. Plasma parameters diagnosis

Optical emission spectroscopy (OES) is a relatively simple but powerful plasma diagnostic method that is non-intrusive and *in-situ*. It has a widespread use in plasma assisted processes in order to identify the atomic and molecular species present in the discharge. Common analysis of plasma with OES is based on the fact that the relative intensities of lines in molecular emission spectra depend on the temperature of the emitting species [44–47].

Optical emission measurements were recorded through an optical access in the center of the waveguide. Two parabolic mirrors imaged the emitted light of the core of the discharge into a narrow-band OceanOptics HRC29301 spectrometer (400-530nm). Acquisition time varied between 10 ms to 1 second, depending on plasma emission intensity. Spectra were corrected for the sensitivity of the CCD (charge-coupled device) array. To find the heavy particle temperature in the plasma, the measured spectra were fitted to synthetic spectra in Lifbase [48] and Specair [49] programs.

For the temperature determination in this work the following transitions were used:

- CH (A-X) system ($A\ ^2\Delta \rightarrow X\ ^2\Pi_r$) 415 nm - 445 nm band,
- C_2 Swan system ($d\ ^3\Pi_g \rightarrow a\ ^3\Pi_u$) 490 nm - 520 nm band.

2.2.4. Parameters describing the reactor's performance

In order to determine the microwave plasma reactor performance basic parameters are defined as follows:

Methane conversion:

$$X_{CH4}\ (\%) = \left(1 - \frac{[CH_4]_{out} \times \upsilon_{out}}{[CH_4]_{in} \times \upsilon_{in}}\right) \times 100 \quad (1)$$

Hydrocarbons selectivity:

$$S_{CxHy}\ (\%) = \left(\frac{x \times [C_xH_y]_{out} \times \upsilon_{out}}{[CH_4]_{in} \times \upsilon_{in} - [CH_4]_{out} \times \upsilon_{out}}\right) \times 100 \quad (2)$$

Hydrocarbons yield:

$$Y_{CxHy}\ (\%) = \frac{X_{CH4}\ (\%) \times S_{CxHy}(\%)}{100} \quad (3)$$

Lack of carbon — the difference between the quantified amount of carbon at the inlet and outlet of the reactor (it corresponds to the yield of all the not quantified carbon-containing products):

$$C\ lack\ (\%) = \left(1 - \frac{\upsilon_{out} \times \sum\left(x \times [C_xH_y]_{out}\right)}{[CH_4]_{in} \times \upsilon_{in}}\right) \times 100 \quad (4)$$

Selectivity of carbon lack:

$$S_{C\ lack}(\%) = \frac{C\ lack\ (\%)}{X_{CH4}\ (\%)} \times 100 \quad (5)$$

Hydrogen selectivity:

$$S_{H2}(\%) = \left(\frac{1}{2} \times \frac{[H_2]_{out} \times \upsilon_{out} - [H_2]_{in} \times \upsilon_{in}}{[CH_4]_{in} \times \upsilon_{in} - [CH_4]_{out} \times \upsilon_{out}}\right) \times 100 \quad (6)$$

Hydrogen yield:

$$Y_{H2}(\%) = \frac{X_{CH4}\ (\%) \times S_{H2}(\%)}{100} \quad (7)$$

Lack of hydrogen — the difference between the quantified amount of hydrogen at the inlet and outlet of the reactor:

$$H\ lack\ (\%) = \left(1 - \frac{\upsilon_{out} \times \sum\left(y \times [C_xH_y]_{out}\right) + \upsilon_{out} \times 2 \times [H_2]_{out}}{4 \times [CH_4]_{in} \times \upsilon_{in} + 2 \times [H_2]_{in} \times \upsilon_{in}}\right) \times 100 \quad (8)$$

Specific energy input (SEI):

$$SEI\ (kJ/mol) = \frac{P \cdot 60 \cdot 22.4}{\upsilon_{in} \cdot 1000} \quad (9)$$

Specific energy requirement (SER):

$$SER\ (kJ/mol) = \frac{P \cdot 60 \cdot 22.4}{([CH_4]_{in} \times \upsilon_{in} - [CH_4]_{out} \times \upsilon_{out}) \cdot 1000} \quad (10)$$

Energy requirement (ER):

$$ER\ (kJ/mol_{C2H2}) = \frac{P \cdot 60 \cdot 22.4}{[C_2H_2]_{out} \times \upsilon_{out} \cdot 1000} \quad (11)$$

where $[C_xH_y]$, $[CH_4]$, $[C_2H_2]$, and $[H_2]$ corresponds to volumetric concentration (%) of the relevant compound, *v* to volumetric flow rate (SLM), *x* to the number of C atoms in a molecule, *y* to the number of H atoms in a molecule, *P* to socket power supplying the MW source (1000 W), and subscripts *in* and *out* refer to the inlet and outlet, respectively. In the case of C lack and H lack calculations, the $[C_xH_y]$ refers to all the quantified hydrocarbons presented in Table 4.

2.2.5. Uncertainty of GC measurement

The GC quantitative analyses involved at least three tests for each sample. The results represent an average value. The uncertainty analysis involved standard deviation, residual standard deviation, and the equipment uncertainty (gas analyzer, gas meter, flow regulators). Concentrations of hydrocarbons other than methane and acetylene were determined based on the acetylene calibration curve, hence these were burdened with an additional error. Based on [43], this was estimated as 5% of the measured value.

3. Theory

3.1. Reactions of methane conversion

The process of methane decomposition, requiring a high temperature (> 1273 K [5]) due to methane's stability [10], can be described with a simplified stepwise reaction (R1):

$$2CH_4 \rightarrow C_2H_6 + H_2 \rightarrow C_2H_4 + 2H_2 \rightarrow C_2H_2 + 3H_2 \rightarrow 2C + 4H_2 \quad \text{(R1)}$$

Since it is a gradual process, the distribution of the products depends on the temperature and reaction time. Many researchers agree that the primary product is C_2H_6, however it is promptly dehydrogenated into further products [5,50]. This phenomenon is mostly affected by the fact that in high temperature (required for sufficient CH_4 conversion rate) the stability of products increases from left to right (in R1) [6,37]. Therefore, long reaction time and high temperature favor the production of unsaturated C_2 compounds, soot, and hydrogen [5,12] with the two latter products being the final one if the conditions are severe enough. Regardless of the products, the decomposition process of methane starts with H abstraction, like in reaction R2, which has a high activation energy and is rate-determining step [50,51]

$$CH_4 \rightarrow CH_3 + H \quad \text{(R2)}$$

The released H radicals play an important and dominant role [27] in further decomposition of methane, accelerating this process due to reaction R3 [5,52].

$$CH_4 + H \rightarrow CH_3 + H_2 \quad \text{(R3)}$$

The CH_3 radical can further dimerize into C_2H_6 or undergo subsequent dehydrogenation, either thermally or by the H abstraction mechanism [38,53] as in R4-5:

$$CH_3 + H \rightarrow CH_2 + H_2 \quad \text{(R4)}$$

$$CH_2 + H \rightarrow CH + H_2 \quad \text{(R5)}$$

Subsequently, the C_2 compounds can be produced through two main pathways: dehydrogenation of ethylene, which might involve the H abstraction mechanism, and CH_x radicals coupling [38,53–55]. Some exemplary reactions of these pathways are presented in Table 2.

Table 2. Exemplary reactions of C_2 compounds creation.

Dehydrogenation of ethylene via H abstraction mechanism	
$C_2H_6 + H \rightarrow C_2H_5 + H_2$	(R6)
$C_2H_5 + H \rightarrow C_2H_4 + H_2$	(R7)
$C_2H_4 + H \rightarrow C_2H_3 + H_2$	(R8)
$C_2H_3 + H \rightarrow C_2H_2 + H_2$	(R9)
Exemplary reactions of CH_x radicals coupling	
$CH_2 + CH_2 \rightarrow C_2H_2 + H_2$	(R10)
$CH + CH_2 \rightarrow C_2H_2 + H$	(R11)
$CH_3 + CH_3 \rightarrow C_2H_4 + H_2$	(R12)
$CH_2 + CH_3 \rightarrow C_2H_4 + H$	(R13)

Additionally, with severe enough conditions, carbon black is produced through intermediate radicals like C, C_2, and C_2H [13,28]. Moreover, the presence of C_xH_y radicals and acetylene can lead to the creation of heavier compounds, e.g. unsaturated C_4 compounds and benzene [13,37,51]. With acetylene and benzene being present in the gas, heavier aromatics and soot can also be found in the methane pyrolysis products, mainly due to the HACA (H-abstraction/C_2H_2-addition) mechanism [13,56,57].

In the case of plasma, the process might be affected not only by the temperature but also by the electrons. A direct electron impact, leading to hydrogen abstraction, requires high-energy electrons (ca. 10 eV) [20] that are not abundant for typical microwave plasma conditions. In fact, the typical energy of electrons in MW plasma is ca. 1 eV, a value that is most suitable for vibrational excitation [55,58]. While it is believed that vibrational excitation of methane may play an important role in its decomposition providing an energetically favorable route, recent research suggests that is not the case for most of the tested plasma reactors, including MW plasma reactors operating at a wide range of pressures [14,15,33]. This process would require highly non-equilibrium plasma with a strong difference between vibrational (T_{vib}) and rotational (T_{rot}) temperatures as well as generally low bulk temperature. In such conditions, the thermal effect is negligible and methane decomposition is driven by electron impact (including vibrational excitation). In the case of MW plasma, that would possibly be achievable by applying extremely low pressure, e.g. 0.1 mbar [33]. In other cases, the vibrationally excited methane molecules are short-living — vibration-translation (V-T) relaxation timescales of CH_4 are circa 2 μs·atm at room temperature [58]. The vibrational energy of methane molecules is promptly lost in vibrational-translational relaxation – a process that is enhanced in higher pressures and temperatures. The energy of the vibrational quanta increases the gas temperature, thereby creating a positive feedback loop: more V-T relaxation gives more heat resulting in even more V-T relaxation [58]. These considerations lead us to believe vibrational excitation to play a minor role in the dissociation process in the conditions given in the presented work.

The influence of hydrogen addition on methane decomposition might be twofold. Firstly, the H radicals have a crucial role in methane decomposition. In fact, in the diamond deposition process, where mixtures of methane highly diluted in hydrogen are used in low pressure MW plasma, reaction R3 is the dominant route leading to methane decomposition [38,59]. This phenomenon can be explained by a high concentration of H radicals (reaching up to 10% [60,61]) and high temperatures in the MW plasma region that affect the reaction R3 (with the reaction rate constant

being T^3 dependent) and a subsequent R4 and R5, resulting in a higher conversion rate of methane and its radicals. Secondly, the dilution with hydrogen suppresses the production of benzene and soot by inhibiting the decomposition of acetylene [37,50,62]. As a result, higher selectivity of acetylene is obtained which is usually accompanied by a higher selectivity of ethylene. It should be noted that this effect was observed in the typical (non-plasma) thermal process of methane decomposition with the temperature range being c.a 1200-2000 K and was accompanied by a decrease in the conversion rate of methane due to reaction reverse to R3. However, this reaction loses its importance in high temperatures (c.a 2500 K) due to the low reaction rate constant [38,62]. Moreover, the effect of soot formation suppression by the presence of hydrogen is also strongly limited in high temperatures [62].

4. Results and Discussion

4.1. Plasma diagnosis

Fig. 2 presents the spectrum of the CH_4-H_2 plasma measured with the HRC29301 spectrometer. It can be seen the dominant emission in the spectrum is from the CH (A-X) system. The other components that are observed in the spectrum are the C_2 Swan system and the H_β line.

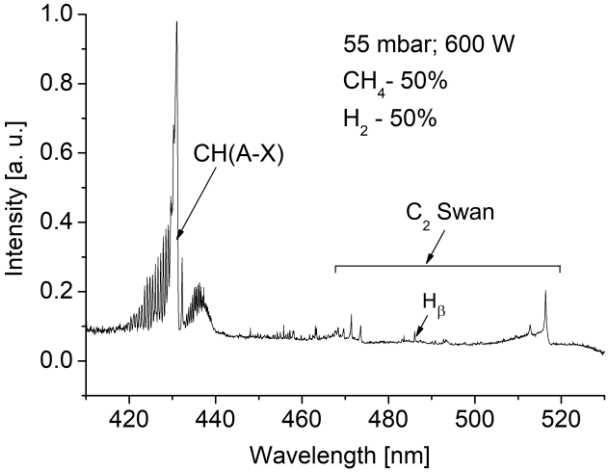

Fig. 2. OES spectrum of CH_4-H_2 plasma (55 mbar, 600 W, measured with OceanOptics HRC29301 spectrometer).

The measured systems were used to determine the rotational and vibrational temperatures. In the case of the CH (A-X) system, the Lifbase [48] software was used (Fig. 3a). For the C_2 Swan (Fig. 3b) the determination of temperatures was done with the Specair [49] program. Determining error margins with unresolved spectra is a complex subject. Errors in CCD calibration and in the applied models (approximation of the slit function, emission coefficients etc.) all play a role in the overall uncertainty. For these measurements we estimate the error on both T_{vib} and T_{rot} to be within 100 K, which is the margin in which satisfactory overlap between synthetic and measured spectra could be achieved. The measured temperatures are collected in Table 3. As it can be seen, T_{rot} is

exceeding 3000 K in all the cases. It should be noted, that rotational-translational relaxation is an extremely fast mechanism occurring on the timescale of a single collision [63]. Considering the radiative lifetimes of the detected C_2 and CH systems are in the range of 0.1-1 μs [64], we can safely conclude T_{rot} of the emitting state to be equal to the gas temperature [38,65]. Another conclusion from the temperature measurements is that the plasma is very close to thermal equilibrium as T_{rot} and T_{vib} show similar values. This is not surprising as the high gas temperature intensifies V-T relaxation [58] as discussed before (Section 3.1). The equilibrated temperatures are especially visible in the C_2 Swan system. In the case of CH (A-X) emission a higher distinction between T_{vib} and T_{rot} is observed. The disagreement between both systems has been described before and was attributed to the different origins of excited species [66]. In the case of C_2 (d) the predominant production mechanism is electronic impact excitation and carbon-atom recombination [64,66,67]. Similarly, CH (A) can be created through collisions with electrons [64] or through chemiluminescent reactions with H_2 (R14) [64,66,68]:

$$C + H_2 \rightarrow CH\ (A) + H \qquad \text{(R14)}$$

It is speculated that the CH (A) can be formed with a high quantum number through reaction R14, analogous to N_2 recombination in plasma, which could in turn explain the higher vibrational temperature of this system [69]. This reasoning would explain why the CH temperature is affected by the H_2 addition and the C_2 temperature is not. Another change with the temperature distribution is associated with the pressure — with increased pressure the difference between CH T_{rot} and T_{vib} is decreasing. This is in good agreement with theory as the collision frequency increases with pressure, thereby intensifying relaxation processes and thus magnifying the thermal equilibrium. Finally, the observed increase in T_{rot} (more evident in the case of CH) might also be attributed to higher power density due to the contraction of the plasma taking place at 110 mbar [42]. As the final remark, it should be noted that the presented temperatures do not include cases with pure methane. This is due to vast amounts of soot-like deposit produced when no hydrogen was added. Consequently, due to strong interferences, the gathered spectra did not allow estimating the temperature reliably. However, as the temperatures determined with the C_2 Swan system do not change with the H_2 addition, it could be safely assumed that these cases should be characterized with similar temperatures.

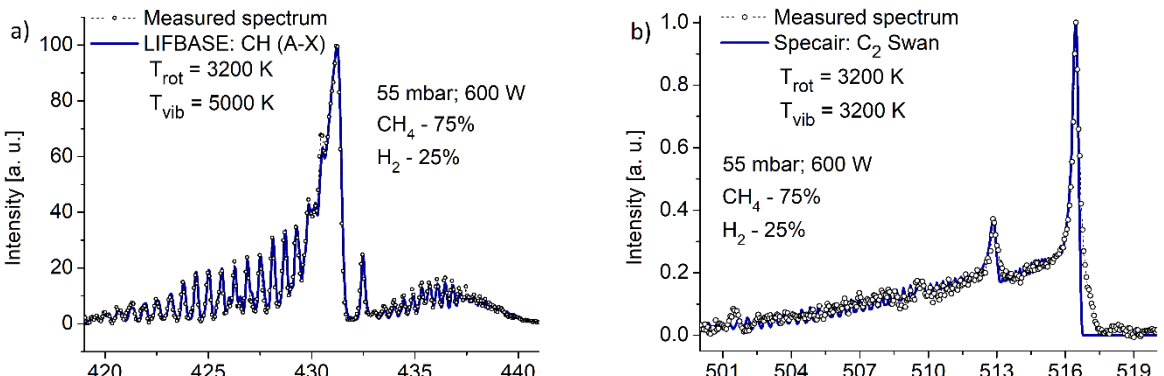

Fig. 3. Comparison of the measured and simulated spectra of CH (A-X) (a) and C_2 Swan (b) systems (55 mbar, 600 W, CH_4:H_2 -3:1 measured with OceanOptics HRC29301 spectrometer).

Table 3. Rotational and vibrational temperatures of different species within the MW plasma.

		CH (A-X)		C_2 Swan	
p, mbar	CH_4:H_2 ratio	415-445 nm		490-520 nm	
		T_{rot}	T_{vib}	T_{rot}	T_{vib}
		K			
55	3:1	3200	5000	3200	3200
	1:1	3000	5000	3000	3400
110	3:1	3500	3500	3300	3300
	1:1	4000	5000	3200	3200

Regardless of the specific particle mechanisms providing the excited species, the most important conclusion from the OES analysis is that the plasma provides high gas temperature and is close to thermal equilibrium. This leads to the conclusion that the chemical processes taking place in the plasma are thermally driven. The same conclusion, based on chemical kinetic modeling of a few plasma reactors (including MW plasma), was presented in the work of A. Bogaerts et al. [14].

4.2. Products of methane conversion

Table 4 presents products from methane coupling obtained in the experiments. Besides these, carbonous soot-like material, negligible amounts of propane and C_4 compounds (2-Butene, 1-Butene or 1-Propene, 2-methyl-), benzene and probably a C_5 unsaturated compound (with m/z of 64) are also produced during the process. While benzene and the C_5 compound were not quantified (as not eluting in the GC-FID column), the high selectivity of acetylene and ethylene, and the high temperature of plasma resulting in the production of soot-like material, suggest that the yield of these compounds is relatively low. It should be noted that some other heavier compounds can also be present as intermediate products in the soot creation pathway.

The products identified in the experiment are in good agreement with the methane decomposition process described in Section 3.1. Due to the high temperature of plasma, the dominant products are acetylene, hydrogen, and soot-like material, which was observed as a black deposit on the reactor's quartz tube. The conversion of methane, along with the concentration of acetylene and hydrogen, is lower in the 55 mbar conditions compared with 110 mbar. On the

other hand, the concentration of ethylene is significantly higher. This phenomenon can be attributed to the lower temperature and shorter expected residence time in the plasma with lower pressure. Similar results were obtained in previous research [10] with the use of the same setup, where a wider spectrum of lower pressures was investigated. It was shown that with the increase in pressure higher conversion rates of methane were achieved and the distribution of the products shifted from ethane to acetylene.

Table 4. Composition of the quantified components from the outlet stream of the MW plasma reactor.

	55 mbar			110 mbar		
	CH_4:H_2 ratio					
	1:0	3:1	1:1	1:0	3:1	1:1
	Concentration (% v/v)					
Methane (CH_4)	55.50±1.13	41.38±1.13	24.94±1.13	51.27±1.13	35.79±1.13	21.18±1.13
Ethane (C_2H_6)	0.19±0.01	0.18±0.01	0.11±0.01	0.07±0.00	0.07±0.00	0.05±0.00
Ethylene (C_2H_4)	1.01±0.09	1.10±0.09	0.88±0.08	0.17±0.01	0.20±0.01	0.22±0.01
Propene (C_3H_6)	0.02±0.00	0.02±0.00	0.01±0.00	0.00±0.00	0.01±0.00	0.01±0.00
Acetylene (C_2H_2)	5.79±0.07	5.32±0.07	5.44±0.07	7.78±0.07	8.18±0.07	7.00±0.07
Allene/Propyne (C_3H_4)	0.08±0.01	0.08±0.00	0.05±0.00	0.05±0.00	0.05±0.00	0.04±0.00
Allene/Propyne (C_3H_4)	0.18±0.01	0.16±0.01	0.10±0.01	0.12±0.01	0.11±0.01	0.08±0.01
C_4[a]	0.03±0.00	0.03±0.00	0.02±0.00	0.01±0.00	0.01±0.00	0.01±0.00
C_4[a]	0.08±0.00	0.07±0.00	0.04±0.00	0.04±0.00	0.03±0.00	0.02±0.00
Diacetylene (C_4H_2)	0.31±0.03	0.19±0.01	0.12±0.01	0.40±0.04	0.35±0.03	0.15±0.01
Hydrogen	28.60±1.15	46.40±1.15	73.10±1.15	30.50±1.15	50.60±1.15	73.00±1.15

[a] - 1-Butyne/2-Butyne/1,2-Butadiene/1,3-Butadiene (C_4H_6)

4.3. Influence of hydrogen addition

The expected beneficial effect of hydrogen addition, described in Section 3.1, was confirmed in the experiments. Fig. 4 shows that the presence of hydrogen in the gaseous mixture significantly increases the conversion rate of methane (calculated as in eq. 1). The increase in conversion rate is 36% and 43% for the pressure of 55 mbar and 110 mbar, respectively. The higher increase obtained in the case of 110 mbar can be attributed to the higher temperature that additionally should result in a higher population of H radicals derived from both methane and hydrogen decomposition [38]. It should be pointed out, that the presence of excited H radicals in the plasma was confirmed with the OES analyses (Section 3.2 – Fig. 2). While the measurements of H lines

emission alone do not provide information about the density of ground state H radicals or their source (whether from CH_4 decomposition of H_2 dissociation) they indicate the presence of atomic hydrogen in the plasma. The high concentration of H radicals through a high H_2 dissociation rate has been proven in diamond deposition experiments conducted in similar conditions to those presented in this work (See Section 3.1). This suggests that the addition of H_2 provides an additional pool of H radicals that play a crucial role in methane decomposition (R3).

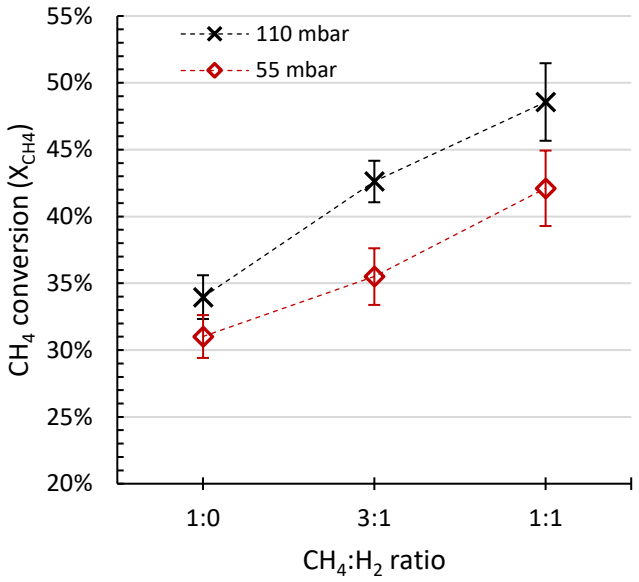

Fig. 4. Conversion rate of methane depending on the pressure and CH_4:H_2 ratio.

Besides increasing the conversion rate of methane, the addition of hydrogen influences the distribution of the products. The higher conversion rate of methane and methane radicals (R3 and R4-5) opens the pathway for dimerization reactions (R10-13). Moreover, the presence of H radicals enhances the important route of ethylene and acetylene creation [38,53], as in R6-9, which are favored at higher temperatures [38]. This results in the increase in acetylene and ethylene yield (calculated as in eq. 3) presented in Fig. 5.

The optical emission, providing information on the temperature and presence of excited H radicals, was collected from the center of the waveguide (Fig. 1), here power is provided and logically temperature and H concentration are the highest. Moving away from the waveguide, both temperature and H radical concentration decrease, thereby making molecular hydrogen the dominant form of hydrogen. Therefore, it can be assumed that the conditions downstream of the plasma begin to resemble the conditions of the typical thermal methane decomposition process. Consequently, the abundance of H_2 can influence the dehydrogenation reactions shifting them to the left (as in R1). This process might explain the increase in selectivity (calculated accordingly to eq. 2) of both ethylene and acetylene (Fig. 6).

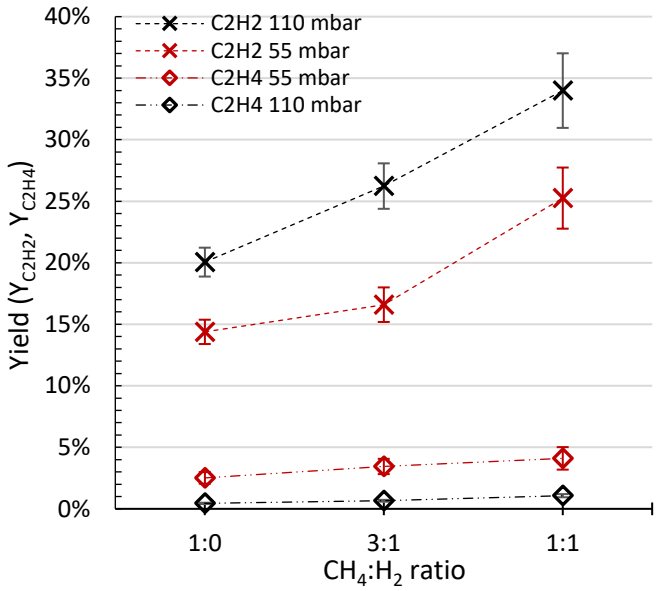

Fig. 5. Yield of ethylene and acetylene depending on the pressure and CH_4:H_2 ratio.

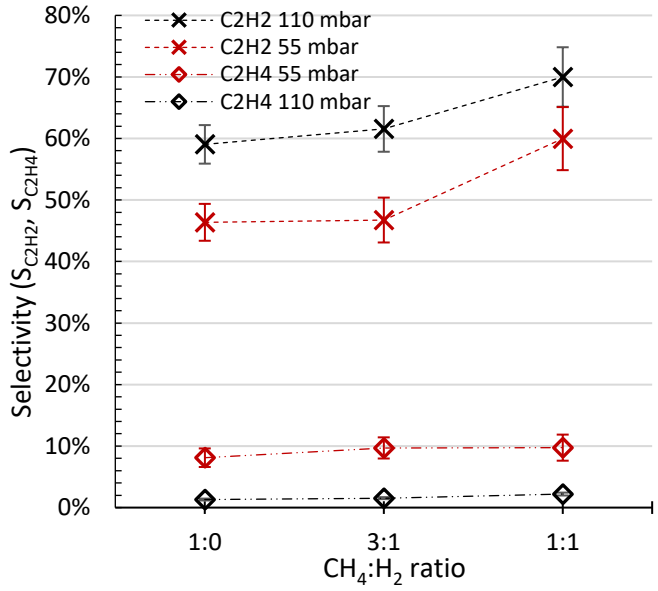

Fig. 6. Selectivity of ethylene and acetylene depending on the pressure and CH_4:H_2 ratio.

When considering the increase in acetylene selectivity, the nature and changes in the soot-like deposit should be discussed. The black carbonous deposit produced in plasma processing of hydrocarbons is a mixture of carbon particles, heavier hydrocarbons, soot, amorphous carbon, and its graphitized structures [56,57]. Therefore, with lighter hydrocarbons being quantified, the C lack can be identified as the yield of a mixture of heavier compounds including aromatic compounds, carbon material, and soot. The C lack, along with H lack, and selectivity of C lack (determined from eq. 4, 5, and 8) is shown in Fig. 7 and 8.

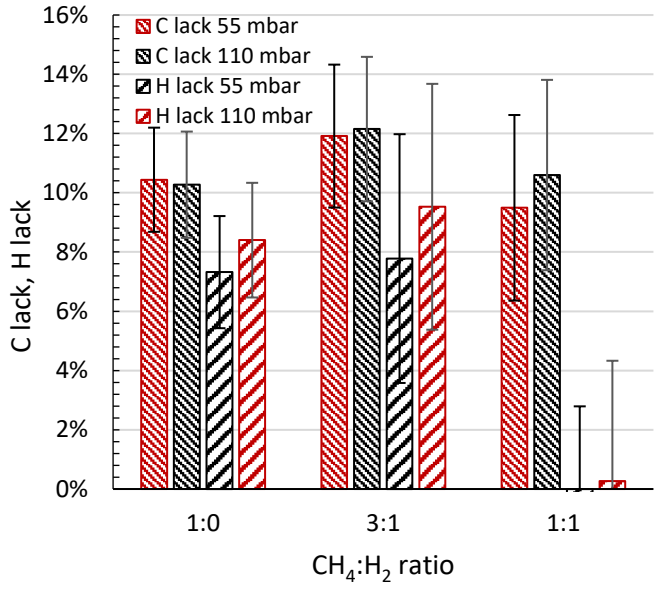

Fig. 7. C lack and H lack depending on the pressure and CH_4:H_2 ratio.

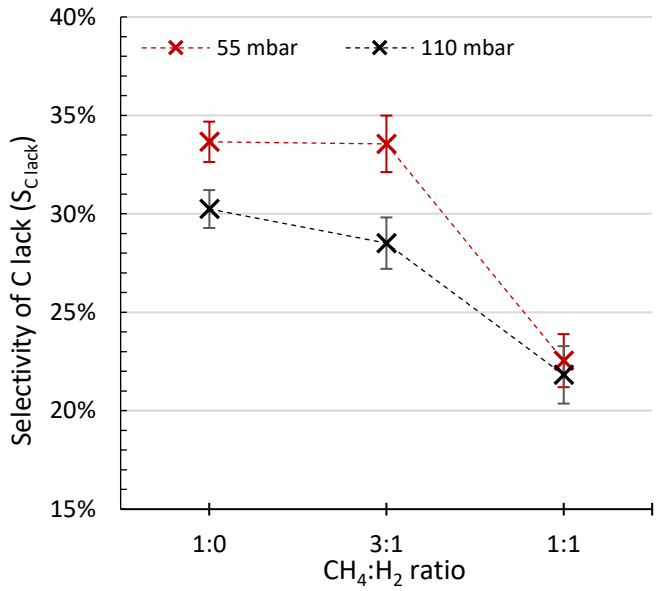

Fig. 8. Selectivity of C lack depending on the pressure and CH_4:H_2 ratio.

As presented, the C lack remains more or less the same within the whole range of tests. However, as the methane conversion increases with the hydrogen addition, the selectivity of C lack decreases. While acetylene is a crucial compound in the formation of all the above mentioned products [28,51,70], its role in the formation of the specific products might be different. The production of heavy aromatic compounds, including polycyclic aromatic hydrocarbons (PAHs), followed by the formation of soot is explained by HACA mechanism [71]. Simplifying, the mechanism can be described as in R15-16:

$$A_i + H \leftrightarrow A_{i-} + H_2 \quad \text{(R15)}$$

$$A_{i-} + C_2H_2 \leftrightarrow A_iC_2H_2 \quad \text{(R16)}$$

where A_i is a molecule consisting of aromatic rings and A_{i-} is its radical derived from H abstraction. As the reaction R15 is reversible, the abundance of molecular hydrogen leads to consumption of aromatic radicals, thereby suppressing reaction R16. Otherwise, acetylene is attached to the aromatic rings in a multistep process that leads to acetylene consumption and aromatic structure growth with soot being the final product. The role of acetylene in soot formation is limited not only to the condensation of aromatic rings, but it also plays a crucial role in the formation of lighter, initial soot precursors as C_2H radicals. Additional hydrogen can, however, lead to the recreation of acetylene, limiting the presence of soot precursors (R17) [13,70]:

$$C_2H + H_2 \rightarrow C_2H_2 + H \quad \text{(R17)}$$

This explains the increase in acetylene selectivity at the cost of PAHs and soot when hydrogen is added. This process is typical for flames and was proved both experimentally and by modeling [71,72]. Therefore, it can be assumed that in the MW plasma reactor it takes place in the downstream part of the reactor. In the upper part of the reactor, aromatic compounds are not yet formed. On the other hand, the high temperature in the core of the MW plasma reactor favors the creation of hydrogen-less carbonous structures, e.g. carbon black, carbon particles, and amorphous carbon, as they may be created via condensation of C and C_2 particles [67,73]. Interestingly, these assumptions seem to be supported by the obtained results. In Fig. 7 and 8, for the case with the highest H_2 addition, the stable C lack is accompanied by the slight decrease in C lack selectivity and a significant decrease in H lack (the H lack corresponds to the hydrogen in the not quantified products – the soot-like deposit). This might be a result of the changes in the distribution of the soot-like product. With the PAHs and soot (containing hydrogen) being suppressed by the hydrogen addition, the formed deposit might consist mainly of hydrogen-less forms of carbon. However, it should be noted that the C lack and H lack determination is overburdened with a high error. More detailed quantitative (possibly direct) and qualitative analyses of the soot-like product should be carried out to prove this assumption. As the final remark considering the soot-like deposit, it should be noted, that while the C lack shows similar values regardless of the CH_4:H_2 ratio, the real amount of produced carbonous material is proportional to the inlet concentration of CH_4. In other words, in the case of ratio 1:1 the output of soot-like deposit is ca. twice smaller than in the case 1:0.

Another indicator showing the shift from heavier compounds to acetylene is diacetylene. Creation of this compound is also strictly connected with acetylene and its radical (C_2H), as in R18 [70]:

$$C_2H_2 + C_2H \rightarrow C_4H_2 + H \quad \text{(R18)}$$

Therefore, hydrogenation of C_2H radical (as in R17) would result in increased selectivity of acetylene at the cost of diacetylene. As presented in Table 4, the concentration of diacetylene is

decreasing with the addition of hydrogen. These values correspond to the decrease in selectivity from 5.04% to 2.64% (for the pressure of 55 mbar and CH_4:H_2 ratio of 1:0 and 1:1, respectively) and from 6.12% to 3.09% (for the pressure of 110 mbar and CH_4:H_2 ratio of 1:0 and 1:1, respectively). Analogically, the yield of diacetylene decreases from 1.56% to 1.11% (55 mbar) and from 2.08% to 1.50% (110 mbar).

Finally, the increase in ethylene selectivity might be explained analogically to acetylene but with the involvement of C_2H_3 radical as in R19:

$$C_2H_3 + H_2 \rightarrow C_2H_4 + H \quad \text{(R19)}$$

While this process is happening at the cost of acetylene (R9), the decrease in its output in not observed due to the simultaneous increase in acetylene yield and selectivity via other, above discussed pathways. The other explanation of ethylene selectivity increase might be due to simple acetylene hydrogenation (as in R20), however, this is an exothermic reaction thus believed to have a marginal influence in the given conditions [53].

$$C_2H_2 + H_2 \rightarrow C_2H_4 \quad \text{(R20)}$$

The final product to consider is hydrogen. The selectivity and yield of H_2, presented in Fig. 9 and calculated accordingly to eq. 6 and 7, follow the same trends as acetylene. This seems logical as the acetylene is produced due to dehydrogenation of methane that leads to H_2 production. As a result, the net output of hydrogen is positive. From the point of the process concept, this would allow to recirculate part of the produced hydrogen back into the process, with the rest being a valuable product on its own. Moreover, with the implementation of a catalyst, it could be also used to hydrogenate acetylene shifting the products into ethylene (R20) [21].

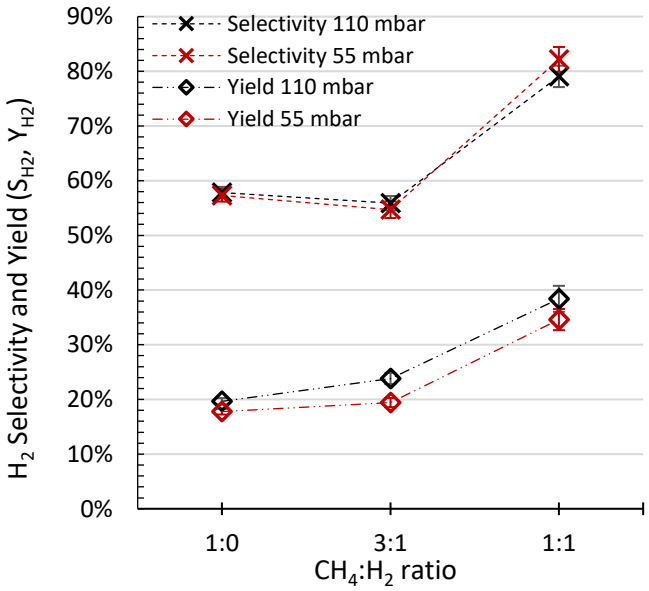

Fig. 9. Yield and selectivity of H_2 depending on the experimental conditions.

As a final remark, it should be noted that the effect resulting from H_2 addition was more evident when the ratio of 1:1 rather then 3:1 was applied. In some cases of the 3:1 ratio tests, the effect of hydrogen addition can be barely noticeable. This can be observed for the selectivity of acetylene and C lack (Figures 6 and 8). Moreover, even a drop in the H_2 selectivity can be observed for the case with the smaller addition of hydrogen (Figure 9). On the other hand, the increase in methane conversion and the resulting increase in the yields (C_2 compounds, C lack, and H_2) are more distinct. This could mean that while the addition of hydrogen with the CH_4:H_2 ratio of 3:1 was enough to enhanced methane conversion, the applied amount of hydrogen was too small to significantly affect the distribution of the products, e.g. through reactions R15 (reversed) and R17. Similarly to the already discussed changes in the nature of soot-like material with the ratio of 1:1, the presence of additional hydrogen in the case 3:1 might have also affected the composition of the soot-like material and the resulting H_2 selectivity. The growth of aromatic structures (that leads to PAHs and soot production) may be exemplary presented as follows: benzene (C_6H_6) → naphthalene ($C_{10}H_8$) → phenanthrene ($C_{14}H_{10}$) → pyrene ($C_{16}H_{10}$). While this process may be accompanied by other mechanisms then HACA, they all involve radicals and a stepwise hydrogen release [74]. The radical propagation of the aromatic structure growth can be terminated by H_2 molecules (reversed R15). Therefore, the additional hydrogen in the case with CH_4:H_2 ratio of 3:1 could have resulted in intensified blocking of the growth pathway, when compared to the case with no hydrogen addition, and preventing condensation of the aromatic structures. Consequently, a higher amount of hydrogen would remain bounded within the aromatic structure rather than being released. That could lead to decreases in the H_2 selectivity. This assumption is in good agreement with the increase in the H lack that was observed for the ratio of 3:1 (Figure 7). As the aromatic compounds were not quantified, the increase in their hydrogen content would result in the observed increase in the H lack. However, it should be noted that the small changes in the results observed for the case with CH_4:H_2 ratio of 3:1 are accompanied with relatively high errors. Consequently, these results are hard to interpret and should be treated with caution. Nevertheless, the trends clearly show that changing the H_2 content from 25% to 50% increases its impact on the process significantly. With overcoming the problems with plasma stability, a higher dilution with hydrogen (e.g. CH_4:H_2 ratio of 2 or 3) should enhance the beneficial effects of hydrogen addition even more, as it was proven in other works [2,3].

5. Energy costs and comparison with other plasma techniques

To determine the energy costs of methane coupling three parameters are used, i.e. specific energy input (SEI), specific energy requirement (SER), and energy requirement (ER), calculated as in eq. 9-11, respectively. The SEI is constant due to the fixed input volumetric gas flow rate (6 SLM) and magnetron power consumption (1000 W) and its value is 224 kJ/mol. The SER and ER are presented in Fig. 10 and 11, respectively. As it can be seen, the SER is gradually increasing with the CH_4:H_2 ratio. As the SER is calculated per converted CH_4 molecule, this decrease is caused by a significant drop in the input CH_4 concentration that is not compensated by the obtained increase in the CH_4 conversion rate. The ER, calculated per produced acetylene molecule, shows rather more fixed values. This can be explained by the fact, that the C_2H_2 yield increase, caused by the addition of H_2, is relatively higher than the increase in the CH_4 conversion. As it was shown in Table 4, the concentration of C_2H_2 is rather constant despite a significant drop in the input CH_4 concentration.

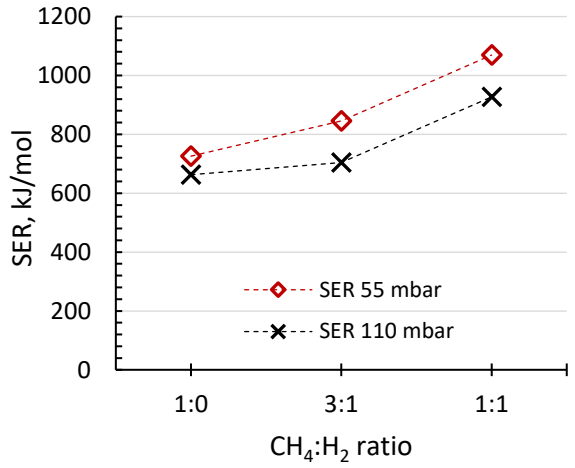

Fig. 10. SER for different CH_4:H_2 ratios in two pressure regimes.

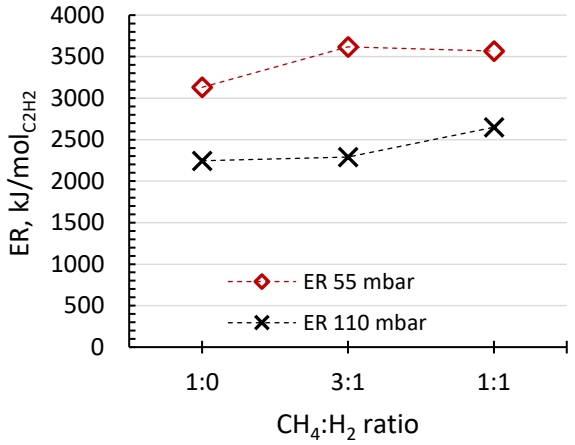

Fig. 11. ER for different CH_4:H_2 ratios in two pressure regimes.

Considering the energy costs parameters, a few issues should be pointed out. First of all, the process was not optimized in any way. The focus in this work was on investigating the effects of

hydrogen addition on the plasma process. The process was conducted in fixed conditions, while changes in all the parameters, i.e. MW input power, pressure, gas flow rate, and CH_4:H_2 ratio would affect the process efficiency and energy cost. Secondly, the calculation of all the three above mentioned parameters do not include the power consumption of the vacuum pump. In the case of presented work, the vacuum pump power consumption is estimated to be ca. 500 W (accordingly to the producer's datasheet) meaning that all the energy parameters would increase by 50%. However, the pump used in the system was not well-fitted to the process requirements. It is designed to work with much higher gas flow rates (with a peak pumping speed of 35 m^3/h). Applying a better-matched vacuum pump should decrease energy consumption significantly. Thirdly, the SER involves only C_2H_2 while the C_2H_4 share is still noticeable (at least in the case of 55 mbar). While this approach is justified by the need of comparing results from different experiments, the real ER should be lower as C_2H_4 is one of the desired products. Finally, the tests involved a 2.45 GHz microwave generator. These types of generators are usually used in a laboratory test due to their high availability, low costs, and suitable power range. However, their energy efficiency is only ca. 60%. On the other hand, 915 MHz generators, usually working in a higher power range, have the energy efficiency of ca. 85%. Applying this kind of a MW generator would result in a significant decrease in energy consumption.

In general, the overall efficiency of the methane coupling process in the moderate pressure MW plasma reactor with the addition of H_2 is somewhere between the results obtained for different kinds of plasmas. Their comparison in the context of methane coupling, based on the review work of Scapinello et al. [5], is presented in Table 5. As can be seen, the conversion rate of methane in the tested MW plasma reactor is higher than in the case of DBD, corona, pulsed discharge, or gliding-arc plasmas, similar to atmospheric MW plasma, and significantly lower than in 30 mbar MW plasma. The SEI is usually higher (but similar for DBD and corona plasma and much lower than in other MW plasmas) yet the SER is lower or similar with exception of PD plasma.

Table 5. Performance of different kinds of plasma reactors. The literature references present the best results achieved [5] while the results from this work(*) present the whole scope of results for two different pressure regimes (55 mbar and 110 mbar) and three CH_4:H_2 ratios (1:0, 3:1, 1:1).

Plasma type	SEI kJ/mol	X_{CH4} %	Selectivity %			SER kJ/mol	ER kJ/mol$_{C2H2}$	Ref.
			C_2H_6	C_2H_4	C_2H_2			
DBD	202	10.5	34	19 (C_2H_2+C_2H_4)		1921	-	[18]
Corona	194	8.5	-	-	76.5	2278	5957	[25]
PD	86	23.5	1.9	5.4	85	365	860	[75]
GA	115	15	2.9	8.7	75	769	2050	[76]

MW	1076	50.7	-	11.5	61.4	2122	6920	[2]
MW (30 mbar)	617	93.7	1.8	9.8	65.3	659	2018	[59]
MW*	224	31.0-48.6	-	1.3-9.7	46.4-70.0	663-1069	2245-3618	This work

6. Conclusions

Methane coupling to valuable C_2 compounds by means of plasma was studied. The focus of this work was the impact of hydrogen addition on the non-oxidative methane coupling in a warm, moderate pressure microwave reactor in two different regimes of radial confinement. Optical emission measurements were coupled with downstream measurements of conversion and product distributions.

The dilution with hydrogen has a twofold beneficial effect. Firstly, it increases the conversion rate of methane and yields of ethylene and acetylene when compared to pure methane plasma. For the CH_4:H_2 ratio of 1:1 the conversion rate increases by ca. 36% and 43% for the pressure of 55 mbar and 110 mbar, respectively. The yield of acetylene increases by ca. 76% and 69%, while the yield of ethylene increases by 64% and 175% for the pressure of 55 mbar and 110 mbar, respectively. Due to the high temperature of the plasma (with the use of OES techniques the rotational temperature of heavy particles was determined to be above 3000 K), the dominant product is acetylene. The product distribution can be shifted towards ethylene by decreasing the pressure. It shortens residence times and changes the plasma shape from radially confined to diffuse which is characterized by a more homogenous discharge with lower gas temperature. Secondly, with the CH_4:H_2 ratio of 1:1 the addition of hydrogen results in an increase in C_2 compounds selectivity at the cost of problematic soot-like product. It is believed that these two effects can be associated with two plasma regions. Close to the center of the plasma, the high concentration of H radicals plays a crucial role in the high-temperature driven process of methane decomposition. Further downstream an abundance of molecular hydrogen leads to suppression of carbonous material deposition, presumably mainly PAHs and soot.

In general, these results have shown that the addition of hydrogen is an easily applicable method for methane coupling improvement in warm plasmas. Overall, the test with hydrogen addition (CH_4:H_2 ratio of 1:1) resulted in a similar output of C_2 compounds as in the case of pure methane, with a twice smaller production of soot-like materials, ca. twice smaller consumption of methane, and a similar energy requirement. With the suppression of soot deposit, this method might be beneficial in terms of hybrid plasma-catalytic systems that are vulnerable to deactivation caused by soot presence. Moreover, it should be noted that hydrogen is one of the main products of the methane coupling process, the yield of which is also enhanced by hydrogen addition resulting in a

positive net output of this product. As the hydrogen needs to be separated from the outlet stream regardless of whether it was initially introduced or not, this creates a simple technological possibility of recirculating part of the produced hydrogen allowing for a more flexible control (along with the possibility to adjust the reactor's pressure) of the process depending on the demanded products. While the work of the reactor was not optimized yet, it shows one of the highest conversion rates of methane when compared to other types of plasma reactors with balanced energy requirement parameters.

Therefore, it is believed that warm plasma coupling of methane into C_2 compounds in the presence of hydrogen might be a promising and flexible way of non-oxidative production of valuable acetylene and ethylene. To establish the conclusion on the dualistic effect of hydrogen addition further work including wider range of H_2:CH_4 ratios, soot-like material analyses, determination of the H radicals density, and modeling of the presented mechanisms should be carried out. Moreover, it should be noted, that while the presented work investigated moderate pressure MW plasma, the discussed process might also be applicable for other warm plasma sources, e.g. atmospheric MW plasma or GA plasma.

Acknowledgments

This work was supported by the Polish Ministry of Science and Higher Education (subvention number 049M/0014/19) and received support from the Netherlands Organization for Scientific Research (NWO) in the framework of the CO2-to-Products program with kind support from Shell, and the ENW PPP Fund for the top sectors.

Declaration of competing interest

The authors declare that they have no known competing financial interests or personal relationships that could have appeared to influence the work reported in this paper.

References

[1] E. Delikonstantis, M. Scapinello, O. Van Geenhoven, G.D. Stefanidis, Nanosecond pulsed discharge-driven non-oxidative methane coupling in a plate-to-plate electrode configuration plasma reactor, Chem. Eng. J. 380 (2020) 122477. doi:10.1016/j.cej.2019.122477.

[2] J.Q. Zhang, Y.J. Yang, J.S. Zhang, Q. Liu, K.R. Tan, Non-oxidative coupling of methane to C_2 hydrocarbons under above-atmospheric pressure using pulsed microwave plasma, Energy and Fuels. 16 (2002) 687–693. doi:10.1021/ef010217u.

[3] C. Shen, D. Sun, H. Yang, Methane coupling in microwave plasma under atmospheric

pressure, J. Nat. Gas Chem. 20 (2011) 449–456. doi:10.1016/S1003-9953(10)60209-5.

[4] M. Młotek, J. Sentek, K. Krawczyk, K. Schmidt-Szałowski, The hybrid plasma-catalytic process for non-oxidative methane coupling to ethylene and ethane, Appl. Catal. A Gen. 366 (2009) 232–241. doi:10.1016/j.apcata.2009.06.043.

[5] M. Scapinello, E. Delikonstantis, G.D. Stefanidis, The panorama of plasma-assisted non-oxidative methane reforming, Chem. Eng. Process. Process Intensif. 117 (2017) 120–140. doi:10.1016/j.cep.2017.03.024.

[6] M. Scapinello, E. Delikonstantis, G.D. Stefanidis, Direct methane-to-ethylene conversion in a nanosecond pulsed discharge, Fuel. 222 (2018) 705–710. doi:10.1016/j.fuel.2018.03.017.

[7] P. Schwach, X. Pan, X. Bao, Direct conversion of methane to value-added chemicals over heterogeneous catalysts : challenges and prospects, Chem. Rev. 117 (2017) 8497–8520. doi:10.1021/acs.chemrev.6b00715.

[8] A. Galadima, O. Muraza, Revisiting the oxidative coupling of methane to ethylene in the golden period of shale gas : A review, J. Ind. Eng. Chem. 37 (2016) 1–13. doi:10.1016/j.jiec.2016.03.027.

[9] J.Y. Lee, W. Jeon, J.W. Choi, Y.W. Suh, J.M. Ha, D.J. Suh, Y.K. Park, Scaled-up production of C_2 hydrocarbons by the oxidative coupling of methane over pelletized $Na_2WO_4/Mn/SiO_2$ catalysts: Observing hot spots for the selective process, Fuel. 106 (2013) 851–857. doi:10.1016/j.fuel.2013.01.026.

[10] T. Minea, D.C.M. van den Bekerom, F.J.J. Peeters, E. Zoethout, M.F. Graswinckel, M.C.M. van de Sanden, T. Cents, L. Lefferts, G.J. van Rooij, Non-oxidative methane coupling to C_2 hydrocarbons in a microwave plasma reactor, Plasma Process. Polym. 15 (2018) 1–16. doi:10.1002/ppap.201800087.

[11] P. Tang, Q. Zhu, Z. Wu, D. Ma, Methane activation: the past and future, Energy Environ. Sci. 7 (2014) 2580–2591. doi:10.1039/c4ee00604f.

[12] Y. Cheng, T. Li, C. Rehmet, H. An, B. Yan, Y. Cheng, Detailed kinetic modeling of chemical quenching processes of acetylene-rich gas at high temperature, Chem. Eng. J. 315 (2017) 324–334. doi:10.1016/j.cej.2017.01.040.

[13] J.R. Fincke, R.P. Anderson, T. Hyde, B.A. Detering, R. Wright, R.L. Bewley, D.C. Haggard, W.D. Swank, Plasma thermal conversion of methane to acetylene, Plasma Chem. Plasma Process. 22 (2002) 105–136. doi:10.1023/A:1012944615974.

[14] S. Heijkers, M. Aghaei, A. Bogaerts, Plasma-based CH_4 conversion into higher hydrocarbons and H2 : modeling to reveal the reaction mechanisms of different plasma sources, J. Phys. Chem. C. 124 (2020) 7016–7030. doi:10.1021/acs.jpcc.0c00082.

[15] Y. Engelmann, P. Mehta, E.C. Neyts, W.F. Schneider, A. Bogaerts, Predicted influence of plasma activation on nonoxidative coupling of methane on transition metal catalysts, ACS Sustain. Chem. Eng. 8 (2020) 6043–6054. doi:10.1021/acssuschemeng.0c00906.

[16] J. Sun, Q. Chen, Kinetic roles of vibrational excitation in RF plasma assisted methane pyrolysis, J. Energy Chem. 39 (2019) 188–197. doi:10.1016/j.jechem.2019.01.028.

[17] S.Y. Liu, D.H. Mei, Z. Shen, X. Tu, Nonoxidative conversion of methane in a dielectric barrier discharge reactor: Prediction of reaction performance based on neural network model, J. Phys. Chem. C. 118 (2014) 10686–10693. doi:10.1021/jp502557s.

[18] C. Xu, X. Tu, Plasma-assisted methane conversion in an atmospheric pressure dielectric barrier discharge reactor, J. Energy Chem. 22 (2013) 420–425. doi:10.1016/S2095-4956(13)60055-8.

[19] A. Górska, K. Krawczyk, S. Jodzis, K. Schmidt-Szałowski, Non-oxidative methane coupling using Cu/ZnO/Al2O3 catalyst in DBD, Fuel. 90 (2011) 1946–1952. doi:10.1016/j.fuel.2010.12.023.

[20] Y. Gao, S. Zhang, H. Sun, R. Wang, X. Tu, T. Shao, Highly efficient conversion of methane using microsecond and nanosecond pulsed spark discharges, Appl. Energy. 226 (2018) 534–545. doi:10.1016/j.apenergy.2018.06.006.

[21] E. Delikonstantis, M. Scapinello, G.D. Stefanidis, Low energy cost conversion of methane to ethylene in a hybrid plasma-catalytic reactor system, Fuel Process. Technol. 176 (2018) 33–42. doi:10.1016/j.fuproc.2018.03.011.

[22] G. SriBala, D. Michiels, C. Leys, K.M. Van Geem, G.B. Marin, A. Nikiforov, Methane reforming to valuable products by an atmospheric pressure direct current discharge, J. Clean. Prod. 209 (2019) 655–664. doi:10.1016/j.jclepro.2018.10.203.

[23] P. Patiño, Y. Pérez, M. Caetano, Coupling and reforming of methane by means of low pressure radio-frequency plasmas, Fuel. 84 (2005) 2008–2014. doi:10.1016/j.fuel.2005.05.005.

[24] A. Beloqui Redondo, E. Troussard, J.A. Van Bokhoven, Non-oxidative methane conversion assisted by corona discharge, Fuel Process. Technol. 104 (2012) 265–270. doi:10.1016/j.fuproc.2012.05.021.

[25] A. Zhu, W. Gong, X. Zhang, B. Zhang, Coupling of methane under pulse corona plasma (I) - In the absence of oxygen, Sci. China, Ser. B Chem. 43 (2000) 208–214. doi:10.1007/BF03027312.

[26] X. Zhu, X. Liu, H.Y. Lian, J.L. Liu, X.S. Li, Plasma catalytic steam methane reforming for distributed hydrogen production, Catal. Today. 337 (2019) 69–75.

doi:10.1016/j.cattod.2019.05.015.

[27] H. Zhang, W. Wang, X. Li, L. Han, M. Yan, Y. Zhong, X. Tu, Plasma activation of methane for hydrogen production in a N_2 rotating gliding arc warm plasma: A chemical kinetics study, Chem. Eng. J. 345 (2018) 67–78. doi:10.1016/j.cej.2018.03.123.

[28] S. Ravasio, C. Cavallotti, Analysis of reactivity and energy efficiency of methane conversion through non thermal plasmas, Chem. Eng. Sci. 84 (2012) 580–590. doi:10.1016/j.ces.2012.09.012.

[29] M. Jasiński, D. Czylkowski, B. Hrycak, M. Dors, J. Mizeraczyk, Atmospheric pressure microwave plasma source for hydrogen production, Int. J. Hydrogen Energy. 38 (2013) 11473–11483. doi:10.1016/j.ijhydene.2013.05.105.

[30] D.H. Lee, K.T. Kim, Y.H. Song, W.S. Kang, S. Jo, Mapping plasma chemistry in hydrocarbon fuel processing processes, Plasma Chem. Plasma Process. 33 (2013) 249–269. doi:10.1007/s11090-012-9407-7.

[31] A. Fridman, Conversion of methane into acetylene and other processes of gas-phase conversion of hydrocarbons in non-thermal plasmas, in: Plasma Chem., Cambridge University Press, 2008.

[32] J. Sun, Q. Chen, Y. Guo, Z. Zhou, Y. Song, Quantitative behavior of vibrational excitation in AC plasma assisted dry reforming of methane, J. Energy Chem. 46 (2020) 133–143. doi:10.1016/j.jechem.2019.11.002.

[33] T. Butterworth, A. Van De Steeg, D. Van Den Bekerom, T. Minea, T. Righart, Q. Ong, Plasma induced vibrational excitation of CH_4 – a window to its mode selective processing, Plasma Sources Sci. Technol. In Press (2020) 1–34.

[34] Q. Xie, F.C. Borges, Y. Cheng, Y. Wan, Y. Li, X. Lin, Y. Liu, F. Hussain, P. Chen, R. Ruan, Fast microwave-assisted catalytic gasification of biomass for syngas production and tar removal, Bioresour. Technol. 156 (2014) 291–296. doi:10.1016/j.biortech.2014.01.057.

[35] G.J. Van Rooij, D.C.M. Van Den Bekerom, N. Den Harder, T. Minea, G. Berden, W.A. Bongers, R. Engeln, M.F. Graswinckel, E. Zoethout, M.C.M. Van De Sanden, Taming microwave plasma to beat thermodynamics in CO_2 dissociation, Faraday Discuss. 183 (2015) 233–248. doi:10.1039/c5fd00045a.

[36] M. Wnukowski, P. Jamróz, Microwave plasma treatment of simulated biomass syngas: Interactions between the permanent syngas compounds and their influence on the model tar compound conversion, Fuel Process. Technol. 173 (2018) 229–242. doi:10.1016/j.fuproc.2018.01.025.

[37] A. Holmen, O. Olsvik, O.A. Rokstad, Pyrolysis of natural gas: chemistry and process concepts,

Fuel Process. Technol. 42 (1995) 249–267. doi:10.1016/0378-3820(94)00109-7.

[38] M. Heintze, M. Magureanu, M. Kettlitz, Mechanism of C_2 hydrocarbon formation from methane in a pulsed microwave plasma, J. Appl. Phys. 92 (2002) 7022–7031. doi:10.1063/1.1521518.

[39] D.C.M. Van Den Bekerom, J.M.P. Linares, T. Verreycken, E.M. Van Veldhuizen, S. Nijdam, G. Berden, W.A. Bongers, M.C.M. Van De Sanden, G.J. Van Rooij, The importance of thermal dissociation in CO_2 microwave discharges investigated by power pulsing and rotational Raman scattering, Plasma Sources Sci. Technol. 28 (2019). doi:10.1088/1361-6595/aaf519.

[40] S.C. Cho, H.S. Uhm, Y.C. Hong, J.H. Kim, Properties of microwave plasma torch operating at a low pressure, Phys. Plasmas. 15 (2008). doi:10.1063/1.2993210.

[41] C. Biegger, Flow and heat transfer investigations in swirl tubes for gas turbine blade cooling, Universität Stuttgart, 2017.

[42] A.J. Wolf, T.W.H. Righart, F.J.J. Peeters, W.A. Bongers, M.C.M. Van De Sanden, Implications of thermo-chemical instability on the contracted modes in CO_2 microwave plasmas, Plasma Sources Sci. Technol. 29 (2020). doi:10.1088/1361-6595/ab5eca.

[43] J.T. Scanlon, D.E. Willis, Calculation of flame ionization detector relative response factors using the effective carbon number concept, J. Chromatogr. Sci. 23 (1985) 333–340. doi:10.1093/chromsci/23.8.333.

[44] P.J. Bruggeman, N. Sadeghi, D.C. Schram, V. Lins, Gas temperature determination from rotational lines in non-equilibrium plasmas: a review, Plasma Sources Sci. Technol. 23 (2014) 023001. doi:10.1088/0963-0252/23/2/023001.

[45] A. Okada, K. Kijima, Measurement of C_2 rotational temperature in Ar–SiH_4–CH_4 inductively coupled plasma flame with Abel inversion, J. Phys. D. Appl. Phys. 35 (2002) 2126–2132. doi:10.1088/0022-3727/35/17/308.

[46] C. Biloiu, X. Sun, Z. Harvey, E. Scime, An alternative method for gas temperature determination in nitrogen plasmas : Fits of the bands of the first positive system $\mathrm{B}^3\Pi_\mathrm{g} \rightarrow \mathrm{A}^3\Sigma_\mathrm{u}^+$, J. Ap. 101 (2007) 073303. doi:10.1063/1.2537448.

[47] V. Chikan, S.R. Leone, Vibrational and rotational distributions of the CH($A^2\Delta$) product of the C_2H + O(^{3}P) reaction studied by Fourier transform visible (FTVIS) emission spectroscopy, J. Phys. Chem. A. 109 (2005) 10646–10653. doi:10.1021/jp053444w.

[48] J. Luque, D.R. Crosley, LIFBASE: Database and Spectral Simulation Program (Version 1.5), SRI International Report MP 99-009, 1999.

[49] C.O. Laux, Radiation and nonequilibrium collisional-radiative models, in: D. Fletcher, J.-M. Charbonnier, G.S.R. Sarma, T. Magin (Eds.), Physico-Chemical Models for High Enthalpy

Plasma Flows, Von Karman Institute for Fluid Dynamics, Rhode-Saint-Genèse, 2002.

[50] O. Olsvik, O.A. Rokstad, A. Holmen, Pyrolysis of methane in the presence of hydrogen, Chem. Eng. Technol. 18 (1995) 349–358. doi:10.1002/ceat.270180510.

[51] A. Cuoci, A. Frassoldati, T. Faravelli, E. Ranzi, A computational tool for the detailed kinetic modeling of laminar flames: Application to C_2H_4/CH_4 coflow flames, Combust. Flame. 160 (2013) 870–886. doi:10.1016/j.combustflame.2013.01.011.

[52] C. Keramiotis, G. Vourliotakis, G. Skevis, M.A. Founti, C. Esarte, N.E. Sánchez, A. Millera, R. Bilbao, M.U. Alzueta, Experimental and computational study of methane mixtures pyrolysis in a flow reactor under atmospheric pressure, Energy. 43 (2012) 103–110. doi:10.1016/j.energy.2012.02.065.

[53] M. Scapinello, E. Delikonstantis, G.D. Stefanidis, A study on the reaction mechanism of non-oxidative methane coupling in a nanosecond pulsed discharge reactor using isotope analysis, Chem. Eng. J. 360 (2019) 64–74. doi:10.1016/j.cej.2018.11.161.

[54] A. Indarto, N. Coowanitwong, J.W. Choi, H. Lee, H.K. Song, Kinetic modeling of plasma methane conversion in a dielectric barrier discharge, Fuel Process. Technol. 89 (2008) 214–219. doi:10.1016/j.fuproc.2007.09.006.

[55] M. Dors, H. Nowakowska, M. Jasiński, J. Mizeraczyk, Chemical kinetics of methane pyrolysis in microwave plasma at atmospheric pressure, Plasma Chem. Plasma Process. 34 (2014) 313–326. doi:10.1007/s11090-013-9510-4.

[56] P. Jamróz, W. Kordylewski, M. Wnukowski, Microwave plasma application in decomposition and steam reforming of model tar compounds, Fuel Process. Technol. 169 (2018) 1–14. doi:10.1016/j.fuproc.2017.09.009.

[57] N.E. Sánchez, Á. Millera, R. Bilbao, M.U. Alzueta, Polycyclic aromatic hydrocarbons (PAH), soot and light gases formed in the pyrolysis of acetylene at different temperatures: Effect of fuel concentration, J. Anal. Appl. Pyrolysis. 103 (2013) 126–133. doi:10.1016/j.jaap.2012.10.027.

[58] T.D. Butterworth, B. Amyay, D. V.D. Bekerom, A. V.D. Steeg, T. Minea, N. Gatti, Q. Ong, C. Richard, C. van Kruijsdijk, J.T. Smits, A.P. van Bavel, V. Boudon, G.J. van Rooij, Quantifying methane vibrational and rotational temperature with Raman scattering, J. Quant. Spectrosc. Radiat. Transf. 236 (2019) 106562. doi:10.1016/j.jqsrt.2019.07.005.

[59] M. Heintze, M. Magureanu, Methane conversion into acetylene in a microwave plasma: Optimization of the operating parameters, J. Appl. Phys. 92 (2002) 2276–2283. doi:10.1063/1.1497457.

[60] Y. Shimizu, Y. Kittaka, A. Nezu, H. Matsuura, H. Akatsuka, Excited state distributions of

hydrogen atoms in the microwave discharge hydrogen plasma and the effect of electron energy probabilistic function, IEEE Trans. Plasma Sci. 43 (2015) 1758–1768. doi:10.1109/TPS.2015.2419224.

[61] L. Mechold, J. Röpcke, X. Duten, A. Rousseau, On the hydrocarbon chemistry in a H_2 surface wave discharge containing methane, Plasma Sources Sci. Technol. 10 (2001) 52–60. doi:10.1088/0963-0252/10/1/308.

[62] H. Drost, H. Klotz, G. Schulz, The influence of hydrogen on the kinetics of plasmapyrolytic methane conversion, Plasma Chem. Plasma Process. 5 (1985) 55–65. doi:https://doi.org/10.1007/BF00567909.

[63] M. Greenspan, Rotational relaxation in nitrogen, oxygen, and air, J. Acoust. Soc. Am. 31 (1959) 155–160. doi:https://doi.org/10.1121/1.1907686.

[64] J. Luque, W. Juchmann, E.A. Brinkman, J.B. Jeffries, Excited state density distributions of H, C, C_2, and CH by spatially resolved optical emission in a diamond depositing dc-arcjet reactor, J. Vac. Sci. Technol. A Vacuum, Surfaces, Film. 16 (1998) 397–408. doi:10.1116/1.581037.

[65] U. Fantz, Basics of plasma spectroscopy, Plasma Sources Sci. Technol. 15 (2006). doi:10.1088/0963-0252/15/4/S01.

[66] S.W. Reeve, W.A. Weimer, Plasma diagnostics of a direct-current arcjet diamond reactor. II. Optical emission spectroscopy, J. Vac. Sci. Technol. A Vacuum, Surfaces, Film. 13 (1995) 359–367. doi:10.1116/1.579365.

[67] N. Bundaleska, D. Tsyganov, A. Dias, E. Felizardo, J. Henriques, F.M. Dias, M. Abrashev, J. Kissovski, E. Tatarova, Microwave plasma enabled synthesis of free standing carbon nanostructures at atmospheric pressure conditions, Phys. Chem. Chem. Phys. 20 (2018) 13810–13824. doi:10.1039/c8cp01896k.

[68] A. Ehbrecht, A. Kowalski, C. Ottinger, Hot-atom chemiluminescence: a beam study of the reactions $C(^3P) + H_2 \rightarrow CH(A^2\Delta, B^2\Sigma^-, C^2\Sigma^+) + H$, Chem. Phys. Lett. 284 (1998) 205–213. doi:https://doi.org/10.1016/S0009-2614(97)01376-6.

[69] H. Brunet, J. Rocca-Serra, Model for a glow discharge in flowing nitrogen, J. Appl. Phys. 57 (1985) 1574–1581. doi:10.1063/1.334473.

[70] Jürgen Warnatz, Radical chemistry in sooting flames, in: J. Lahaye, G. Prado (Eds.), Soot Combust. Syst. Its Toxic Prop., Springer, Boston, MA, 1983: pp. 127–143. doi:doi.org/10.1007/978-1-4684-4463-6.

[71] S.H. Park, K.M. Lee, C.H. Hwang, Effects of hydrogen addition on soot formation and oxidation in laminar premixed C_2H_2/air flames, Int. J. Hydrogen Energy. 36 (2011) 9304–

9311. doi:10.1016/j.ijhydene.2011.05.031.

[72] S. De Iuliis, S. Maffi, F. Migliorini, F. Cignoli, G. Zizak, Effect of hydrogen addition on soot formation in an ethylene/air premixed flame, Appl. Phys. B Lasers Opt. 106 (2012) 707–715. doi:10.1007/s00340-012-4903-2.

[73] R.C. Bansal, J.-B. Donnet, Formation of soot precursors, in: R.C. Bansal, J.-B. Donnet, M.-J. Wang (Eds.), Carbon Black Sci. Technol., Second Edi, Routledge, Boca Raton, 2018.

[74] B. Shukla, M. Koshi, A novel route for PAH growth in HACA based mechanisms, Combust. Flame. 159 (2012) 3589–3596. doi:10.1016/j.combustflame.2012.08.007.

[75] S.L. Yao, E. Suzuki, N. Meng, A. Nakayama, A high-efficiency reactor for the pulsed plasma conversion of methane, Plasma Chem. Plasma Process. 22 (2002) 225–237. doi:10.1023/A:1014843425384.

[76] N. Rueangjitt, T. Sreethawong, S. Chavadej, H. Sekiguchi, Non-oxidative reforming of methane in a mini-gliding arc discharge reactor: Effects of feed methane concentration, feed flow rate, electrode gap distance, residence time, and catalyst distance, Plasma Chem. Plasma Process. 31 (2011) 517–534. doi:10.1007/s11090-011-9299-y.